ARTICLES

Production of Free Radicals and Triplets from Contact Radical Pairs and from Photochemically Generated Radical Ions

V. S. Gladkikh, G. Angulo, and A. I. Burshtein*

Weizmann Institute of Science, Rehovot 76100, Israel

Received: December 6, 2006; In Final Form: January 24, 2007

The quantum yields of triplets and free radicals (or radical ions) that escaped recombination in photochemically created primary radical pairs (or radical ion pairs) are calculated. As the products of monomolecular photodissociation, the neutral radicals appear at contact, while the ions are initially distributed over the space due to distant photoionization (bimolecular electron transfer) in the liquid solution. The diffusional dependence of the quantum yields is shown to be different when recombination starts from contact or from separated reactants. The experimental data for recombination of ionized perylene with aromatic amine counterions is well fitted with the noncontact initial distribution provided the recombination is also noncontact and even more distant than ionization.

I. Introduction

The formation of free ions and triplets due to recombination/separation of photochemically created radical ion pairs (RIPs) was the subject of the numerous investigations starting from the classical works of Weller and his co-workers.[1−7] The yields of recombination products are very specific functions of encounter diffusion, which were first given analytic interpretation in ref 8. This theory was reasonably well fitted to the experimental data assuming that the recombination is contact and the counterions are initially separated by a definite distance, r_0. The system studied is excited perylene (A*) quenched by electron transfer to some aromatic amines (D). The subsequent incoherent spin conversion proceeding with the rate k_s[9] makes possible the RIP recombination to both the singlet and triplet neutral products accompanied by RIP separation, according to the following comprehensive scheme:

$$\begin{array}{ccccc} & & A^- + D^+ & & \\ & \nearrow & \bar{\varphi} & \searrow & \\ {}^1A^* + D & \xrightarrow{W_I} & {}^1[A^- \ldots D^+] & \underset{k_s}{\overset{3k_s}{\rightleftarrows}} & {}^3[A^- \ldots D^+]\,. \\ \downarrow \tau & & \Downarrow W_S & & \Downarrow W_T \\ A & & [A \ldots D] & & [{}^3A^* \ldots D] \end{array} \qquad (1.1)$$

Here the rate of ionization, $W_I(r)$, as well as the rates of recombination through the singlet and triplets channels, $W_S(r)$ and $W_T(r)$, are space dependent. τ is the excitation life time and the charge separation yield, $\bar{\varphi}(r)$, is averaged over the initial distribution of charges, $f_0(r)$:

$$\bar{\varphi} = \int \varphi(r) f_0(r)\, \mathrm{d}^3 r \qquad (1.2)$$

Setting $f_0(r) = \delta(r - r_0)$, one can calculate the yield of the charge separation from any given starting point, $\varphi(r_0)$. It is very specific for any r_0 and quite different from $\bar{\varphi}$. The same is true for the partial yields of the singlet and triplet recombination and related to their efficiencies. For the averaged yields, these relationships are given by the following formulas:

$$\bar{\varphi} = \frac{\tilde{D}}{Z + \tilde{D}}; \quad \bar{\varphi}_S = \frac{Z_S}{Z + \tilde{D}}; \quad \bar{\varphi}_T = \frac{Z_T}{Z + \tilde{D}} \qquad (1.3)$$

where Z_S and Z_T are the efficiencies of recombination to the singlet and triplet products, whereas

$$Z = Z_S + Z_T$$

is the total one, and $\tilde{D}$ is the counterion diffusion coefficient. As is known,[10]

$$\bar{\varphi} + \bar{\varphi}_S + \bar{\varphi}_T = 1 \qquad (1.4)$$

This relationship holds also for any particular starting distance r_0, including the contact one.

The difference between the charge separation from contact, $\varphi(\sigma)$, and from the remote start, $\bar{\varphi}$, should be especially emphasized. The latter is averaged over the true distribution $f_0(r)$, prepared by preceding photoionization. There is a similar difference between the yields of singlet and triplet neutral products, $\varphi_s(\sigma)$ and $\varphi_t(\sigma)$, and their averaged values, $\bar{\varphi}_s$ and $\bar{\varphi}_t$. The same is true for the corresponding recombination efficiencies.

In principle, the contact yields, $\varphi_s(\sigma)$, $\varphi_t(\sigma)$, and $\varphi(\sigma)$, are worthy of study in their own right. They are the true yields of the photodissociation products provided the excited molecule separates into two contact born radicals: A + $h\nu$ → A* →

10.1021/jp068375f CCC: $37.00 © 2007 American Chemical Society
Published on Web 04/18/2007

[$\dot{B}\cdots\dot{C}$]. However, the same description of the photoionization (eq 1.1) serves only as a useful model for understanding the problem. For the real fitting, all the yields should be averaged over the preliminary calculated initial distribution of the partners in the geminate pairs.

To calculate $\varphi(\sigma)$ and $\varphi_t(\sigma)$ or $\bar{\varphi}$ and $\bar{\varphi}_t$, we have to use the results obtained in ref 8 for the contact recombination in polar solvents (with Onsager radius $r_c = e^2/(\epsilon T) < \sigma$):

$$\varphi_t(r) = k_c^T \frac{3\sigma}{4r} \frac{\alpha k_D + [1 - e^{-\alpha(r-\sigma)/\sigma}](k_D + k_c^S)}{[k_D(1+\alpha) + k_c^T](k_D + k_c^S) + \frac{3}{4}\alpha k_D(k_c^T - k_c^S)} \quad (1.5a)$$

$$\varphi(r) = 1 - \frac{k_c^S/(4\pi r\tilde{D}) + (1 - k_c^S/k_c^T)\varphi_t(r)}{1 + k_c^S/k_D} \quad (1.5b)$$

Here $\alpha = \sqrt{4k_s\sigma^2/\tilde{D}}$ is a measure of the singlet−triplet conversion during encounter time $\sigma^2/\tilde{D}$, and $k_D = 4\pi\sigma\tilde{D}$ is the diffusional rate constant. The double-channel contact recombination, proceeding at only the closest approach distance σ, is represented by two rate constants,

$$k_c^S = \int W_S(r)\, d^3r \quad \text{and} \quad k_c^T = W_T(r)\, d^3r$$

They depend on the free energies of electron transfer to the singlet and triplet products and the electron coupling between the corresponding states.

Assuming recombination to be contact, eqs 1.5a,b were used to obtain the yields and recombination efficiencies at the contact (section II) start. For a remote start, the initial distributions of ions, $f_0(r,\tilde{D})$, have to be calculated for any $\tilde{D}$. This is done by means of differential encounter theory (DET)[10] in section III using the exponential model for the ionization rate:

$$W_I(r) = W_i \exp[-2(r - \sigma)/l_I] \quad (1.6)$$

In section IV, the distributions obtained for such a rate were used for averaging the yields according to recipe 1.2. At small $\tilde{D}$, the diffusional acceleration of the recombination due to a remote start was confirmed for fixed $r_0 \gg \sigma$, as well as for the distributed initial separation. In any case, the theory of contact recombination fits the experimental data only qualitatively, leaving unexplained the diffusional deceleration of recombination at the highest $\tilde{D}$.

The quantitative agreement is reached only in section V, where the exponential rate model is substituted for the contact one, also for recombination:

$$W_S(r) = W_s \exp[-2(r - \sigma)/l_R] \quad \text{and}$$
$$W_T(r) = W_t \exp[-2(r - \sigma)/l_R] \quad (1.7)$$

Then the diffusional deceleration of the recombination is naturally explained. This unexpected effect obtained by Dr. Angulo was first given a proper interpretation in ref 11 using the rectangular model of the recombination rate or its Marcus analog in the deeply inverted region. This effect was attributed to the escape from the extended recombination layer when the start is taken from inside it.[11−13] The spin conversion and recombination through the triplet channel were ignored in these works dealing with single channel recombination. Conversely, the treatment of spin effects in ref 8 was done using the contact model of recombination, which excludes the possibility of an inner start. Here we obtain the same effect once again employing the exponential approximation for both the ionization and recombination rates, eqs 1.6 and 1.7. This helps us to reach the best fit to the experimental data of the total efficiency of recombination, as well as of partial ones, to singlet and triplet recombination products.

II. Contact Start and Contact Recombination

Setting $r = \sigma$, we obtain from eq 1.5:

$$\varphi_t(\sigma) = \frac{3}{4}\alpha \frac{k_c^T k_D}{[k_D(1+\alpha) + k_c^T](k_D + k_c^S) + \frac{3}{4}\alpha k_D(k_c^T - k_c^S)} \quad (2.1a)$$

$$\varphi(\sigma) = \frac{1}{1 + k_c^S/k_D} - \frac{1 - k_c^S/k_c^T}{1 + k_c^S/k_D}\varphi_t(\sigma) \quad (2.1b)$$

If there is no spin conversion, $\varphi_t(\sigma) = \alpha = 0$ but

$$\varphi(\sigma) = \frac{1}{1 + k_c^S/k_D} = \frac{1}{1 + Z/D}, \quad \text{so that} \quad Z = \frac{k_c^S}{4\pi\sigma} = z_s \quad (2.2)$$

These are the conventional results of the spin-less theory,[10] and the same gains from eq 2.1 in the exceptional case $k_c^T = k_c^S$, though the triplet yield is not zero in such a case:

$$\varphi_t(\sigma) = \frac{3}{4}\alpha \frac{k_c k_D}{[k_D(1+\alpha) + k_c](k_D + k_c)} \quad \text{at} \quad k_c^T = k_c^S = k_c \quad (2.3)$$

From the general expression for Z_T and Z_S derived in ref 8 (eq 3.2), we can specify $Z = Z_T + Z_S$ as well:

$$\frac{Z_T}{\tilde{D}} = \frac{3\alpha}{4} \frac{k_c^T}{k_c^T + k_D(1+\alpha)} \quad (2.4a)$$

$$\frac{Z}{\tilde{D}} = \frac{k_c^S}{k_D}\left[1 + \frac{3\alpha}{4} \frac{k_D(1 - k_c^T/k_c^S)}{k_c^T + k_D(1+\alpha)}\right] \quad (2.4b)$$

It is remarkable that Z_T does not depend on the rate of the singlet recombination; it remains invariant at different k_c^S, unlike Z. The total efficiency changes with k_c^S at any $\tilde{D}$ except the borders (at $\tilde{D} = 0$ and $\tilde{D} = \infty$) where always $Z_T = 0$ and $Z = Z_S = z$ (Figure 1). In accordance with eq 2.4b, there is also constant $Z \equiv z$ at any $\tilde{D}$ if $k_c^S = k_c^T$ (horizontal line) and the curvature sign of $Z(\tilde{D})$ is the opposite for $k_c^S < k_c^T$ and $k_c^S > k_c^T$ (upper and lower curves).

For understanding better the physics that is behind the triplet efficiency (eq 2.4a), let us represent it like some "in-cage recombination constant" for the backward electron transfer, k_{bet}, keeping in mind that $\varphi = 1/(1 + Z/\tilde{D}) = 1/(1 + k_{bet}/k_D)$ while $k_{bet} = k_{bet}^T + k_{bet}^S$ and

$$k_{bet}^T = 4\pi\sigma Z_T = \frac{3}{4}\alpha \frac{k_c^T k_D}{k_c^T + k_D(1+\alpha)} = \begin{cases} \frac{3}{4}\alpha k_D & \text{at } k_D/k_c^T \ll 1/\kappa \\ \frac{3}{4}\frac{\alpha}{1+\alpha}k_c^T & \text{at } k_D/k_c^T \gg 1/\kappa \end{cases} \quad (2.5)$$

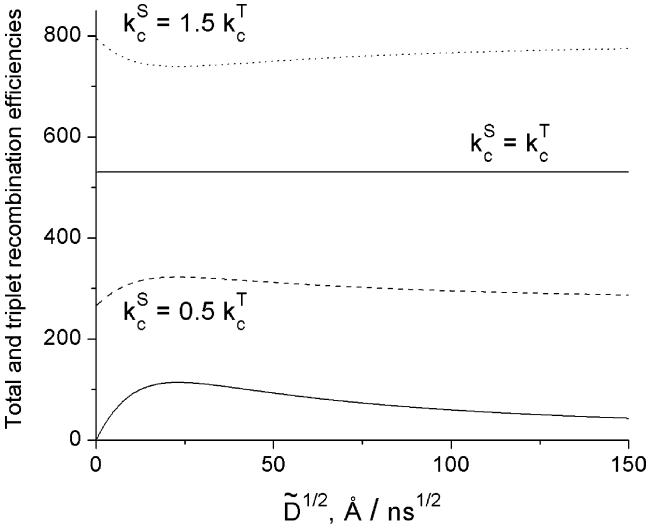

Figure 1. The total recombination efficiency, Z (upper curves), and the triplet one, Z_T (the lowest curve), shown for $k_c^S = k_c^T$ (—), $k_c^S = 0.5\ k_c^T$ (– – –), and $k_c^S = 1.5k_c^T$ (•••) at $k_c^T = 5 \times 10^4$ Å^3/ns.

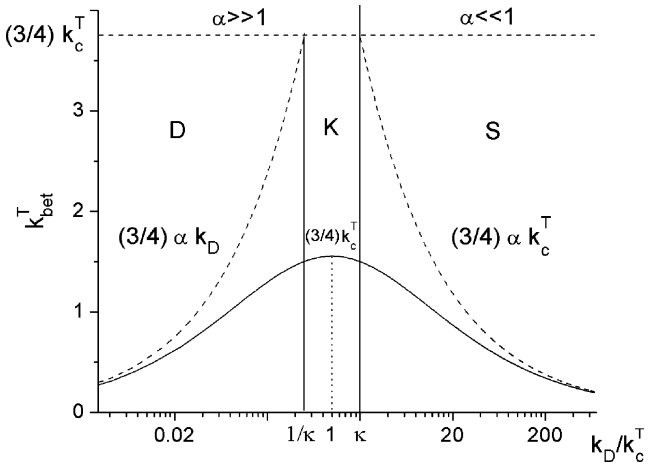

Figure 2. The diffusional dependence of the triplet "in-cage recombination constant" at fast spin conversion ($\kappa = 2$), shown by a solid curve, and the lowest order approximations to this dependence in diffusional (D), kinetic (K), and spin-conversion controlled (S) regions (dashed lines). The solid vertical lines mark the boundaries between these regions, while the dotted line indicates the position of the maximum.

where $\kappa = 16\pi\sigma^3 k_s/k_c^T$ is a measure of the relative spin-conversion strength.

In Figure 2, the diffusional dependence of k_{bet}^T is shown for the fast spin conversion ($\kappa > 1$). In this limit, there are three distinguishable regions: diffusional (D), kinetic (K) and spin-conversion controlled (S). In each of them, the approximate expressions for k_{bet}^T, deduced from eq 2.5, are exposed. Although the start is taken from contact, the radicals are immediately separated and do not recombine until the next recontact and the sequence of subsequent ones. The sooner they follow each other, the faster geminate recombination is accelerated by the diffusion:

$$k_{bet}^T = \frac{3}{4}\alpha k_D = 6\pi\sigma^2\sqrt{k_s\tilde{D}} \quad \text{diffusional limit:} \quad \frac{k_D}{k_c^T} \ll \frac{1}{\kappa} \ll 1 \tag{2.6}$$

When the diffusion becomes too fast, the diffusional control gives way to kinetic control with

$$k_{bet}^T = \frac{3}{4}k_c^T \quad \text{kinetic limit:} \quad \frac{1}{\kappa} \ll \frac{k_D}{k_c^T} \ll \kappa \quad \text{but} \quad \alpha \gg 1 \tag{2.7}$$

This constant value is an upper limit for k_{bet}^T, which is hardly attainable. When diffusion increases, the spin conversion becomes inefficient ($\alpha \ll 1$) and starts to control recombination:

$$k_{bet}^T = \frac{3}{4}\alpha k_c^T = \frac{3}{4}k_c^T\sqrt{\frac{4k_s\sigma^2}{\tilde{D}}} \quad \text{spin conversion control:} \quad \alpha \ll 1 \quad \text{at} \quad \frac{k_D}{k_c^T} \gg \kappa \tag{2.8}$$

Generally speaking the side regions of the diffusional and spin-conversion control extend toward each other, when k_s (as well as κ) reduces. At very slow spin conversion ($\kappa \ll 1$), the intermediate kinetic region is expelled entirely as shown in Figure 3. Simultaneously the maximal k_{bet}^T located at $k_D/k_c^T = 1$ decreases:

$$\max k_{bet}^T = \frac{3}{4}k_c^T\frac{\sqrt{\kappa}}{2+\sqrt{\kappa}} = \begin{cases} \frac{3}{4}k_c^T & \text{at } \kappa \gg 1 \\ \frac{3}{2}\sqrt{\pi\sigma^3 k_s k_c^T} & \text{at } \kappa \ll 1 \end{cases} \tag{2.9}$$

When $k_s \to 0$, the maximum turns to 0 and the whole curve disappears. Such a transformation qualitatively coincides with that studied previously in ref 14 and reviewed in ref 10 (Figure 66). The only distinction is that previously the RIP was created in the triplet state and recombined due to the spin conversion via the permitted singlet channel, while now the process is going back to front.

Another difference is in that here we consider the double channel recombination, looking for both the singlet and triplet channel efficiencies. It is true that the latter does not depend on how strong the former is but not vice versa. If one changes k_c^T, then not only Z_T but also Z_S as well as Z change simultaneously. This is demonstrated in Figure 4, where Z and Z_T are plotted as functions of $\sqrt{\tilde{D}}$ but contrary to Figure 1,

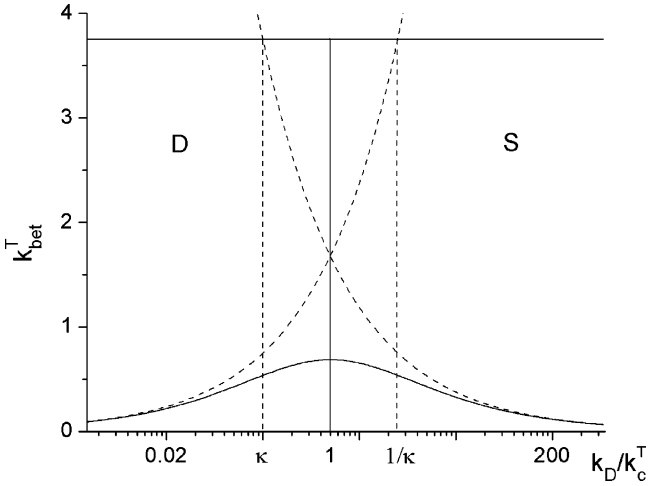

Figure 3. The diffusional dependence of the triplet "in-cage recombination constant" at ten times slower spin conversion than that in Figure 2 ($\kappa = 16\pi\sigma^3 k_s/k_c^T = 0.2$), shown by a solid curve, and the lowest order approximations to this dependence in diffusional (D) and spin-conversion controlled (S) regions (dashed lines). The solid vertical line marks the boundaries between these regions.

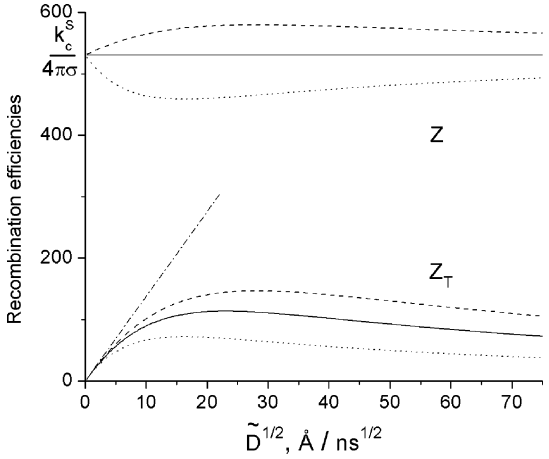

Figure 4. The total (above) and triplet (below) recombination efficiencies at fixed $k_c^S = 5 \times 10^4$ Å^3/ns but different $k_c^T = k_c^S$ (—) as well as for lower $k_c^T = 0.5k_c^S$ (···) and for the larger $k_c^T = 1.5k_c^S$ (— — —). The slope of all triplet curves at $\tilde{D} = 0$ is shown by the dashed-dotted (—·—) straight line.

now k_c^S is kept constant while k_c^T varies. It is remarkable that at these coordinates the linear asymptote of Z_T at $\sqrt{\tilde{D}} \rightarrow 0$, shown by the dashed-dotted line in Figure 4, has the same slope for any k_c^T:

$$Z_T \rightarrow \frac{3}{4}\alpha\tilde{D} = \theta\sqrt{\tilde{D}} \quad \text{where} \quad \theta = \frac{3}{2}\sigma\sqrt{k_s} \qquad (2.10)$$

If such a slow diffusion is attainable, it is easy to find from θ the rate of the spin conversion, k_s, while $Z(0)$ provides us with k_c^S and the argument for maximal Z_T with k_c^T. Having the latter, one can also extract κ from the height of the maximum (eq 2.9) and use it to find $k_s = \kappa k_c^T/(16\pi\sigma^3)$. The low diffusion region is not reachable.

The total recombination efficiency $Z =$ const if $k_c^S = k_c^T$ but has a positive curvature if $k_c^S < k_c^T$ and negative in the opposite case. Unlike Z_T, the total recombination efficiency Z is never zero as $\tilde{D} \rightarrow 0$, unless the radicals start from the contact.

III. Distribution of Initial Separations of Counterions

The diffusional dependence of Z is qualitatively different when the RIPs are the products of bimolecular plotoionization. The electron transfer proceeding with the space-dependent ionization rate, $W_I(r)$, results in some distribution of RIP over interion distances, $m_0(r)$, which is farther from contact the slower is the encounter diffusion of neutral reactants, D. The actual shape of it is given by DET:[15,16]

$$m_0(r) = W_I(r) \int_0^\infty n(r,t)N(t)\, dt \qquad (3.1)$$

In polar solvents, the distribution of reactants, $n(r,t)$, obeys the following equation[17,18]

$$\dot{n} = -W_I(r)n(r,t) + \frac{D}{r^2}\frac{\partial}{\partial r}r^2\frac{\partial n}{\partial r} \qquad (3.2)$$

with reflecting boundary condition

$$4\pi D r^2 \frac{\partial n}{\partial r}\bigg|_{r=\sigma} = 0 \quad \text{and initial one,} \quad n(r,0) = 1 \qquad (3.3)$$

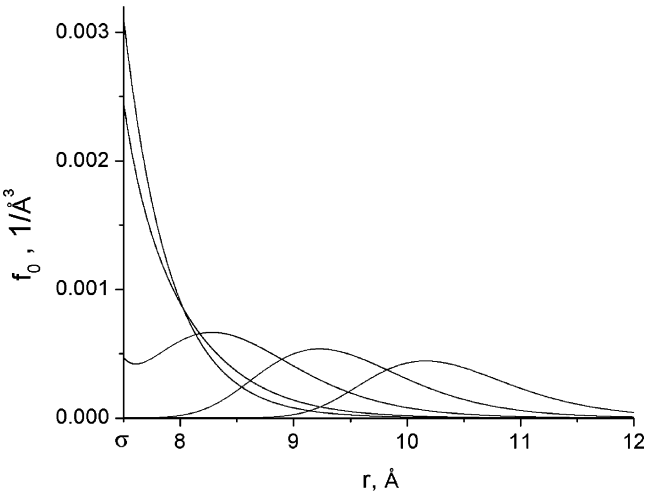

Figure 5. The initial RIP distributions resulting from the exponential ionization with $W_i = 29.12$ ns^{-1} and $l_I = 0.81$ Å at different encounter diffusions of neutral precursors: $D = 10^{-4}$, 10^{-6}, 10^{-7}, 10^{-8}, or 10^{-9} cm^2/s (from left to right).

whereas the quenching kinetics is given by the expression

$$N(t) = \exp\{-t/\tau - c\int d^3r\, W_I(r) \int_0^t n(r,t')\, dt'\} \qquad (3.4)$$

The normalized initial distributions

$$f_0(r) = \frac{m_0(r)}{\int m_0(r)\, d^3r} \qquad (3.5)$$

depend on diffusion and the shape of $W_I(r)$.[10,19] For ionization in the normal Marcus region, the exponential model (eq 1.6) is rather a good approximation. It was used in our calculations performed with the SSDP2 program.[20] The family of initial RIP distributions that are obtained is shown in Figure 5 and confirms once again that at faster diffusion the ions are born closer to the contact distance σ. As $D \rightarrow \infty$, the closest distribution takes the shape that $W_I(r)$ has.

The starting distance averaged over such distributions

$$\bar{r} = \int r f_0(r)\, d^3r \qquad (3.6)$$

decreases with D until ionization is diffusional, but with $D \rightarrow \infty$ it approaches $\bar{r}_{min}$ and remains constant being under kinetic control (Figure 6). Although in this limit $f_0(r)$ coincides in shape with $W_I(r)$, the minimal separation calculated from eq 1.6 is still larger than the contact distance: $\bar{r}_{min} \approx \sigma + l/2$.

IV. Remote Start and Contact Recombination

Since initially the photogenerated ions are always separated (at least by $l/2$), it takes them some time to reach the contact and recombine there. This time is shorter the faster is (at $D \rightarrow \infty$) diffusion of (at $D \rightarrow \infty$) ions, which facilitates the recombination from the remote start.[10,19] In such a case, the total recombination efficiency Z increases with small $\tilde{D}$, instead of being quasi-constant at the contact start considered in the previous section. In particular, at $k_c^S = k_c^T = k_c$, it is a true constant $Z = k_c/(4\pi\sigma)$, shown in Figure 7 by the horizontal dashed line, while Z obtained for the noncontact start (even from the minimal separation $\bar{r}_{min}$) is qualitatively different. It grows with $\tilde{D}$ until recombination is diffusional (region D) and approaches the constant but lower value $Z = k_c/(4\pi\bar{r}_{min})$, when it becomes kinetic (region K). The triplet efficiency Z_T does

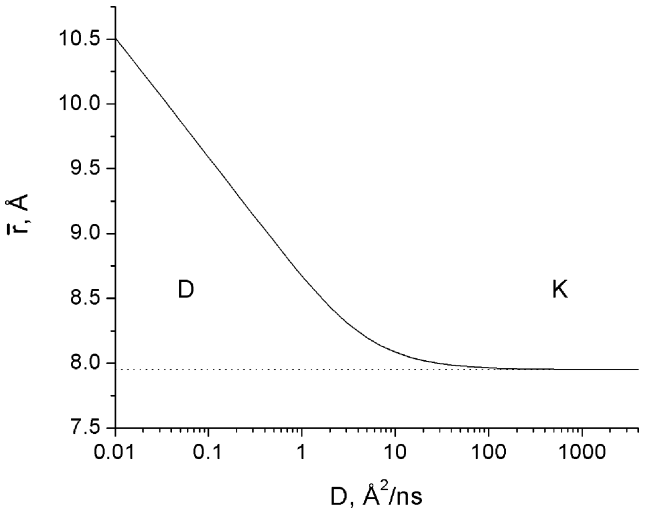

Figure 6. The average initial RIP separation at different encounter diffusion. In region D, where $\bar{r} > \bar{r}_{min}$, diffusion controls ionization, whereas in region K, where ionization is kinetic, the separation becomes minimal: $\bar{r} \approx \bar{r}_{min} = 7.95$ Å.

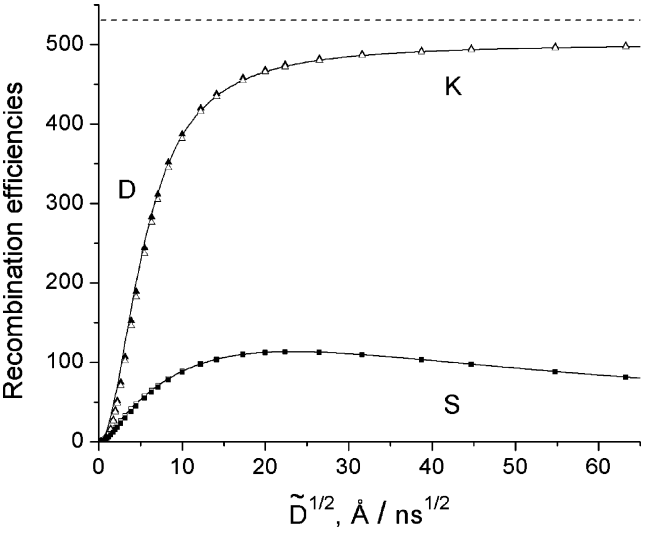

Figure 7. The efficiencies of recombination from different starts at $k_c^S = k_c^T = k_c = 5 \times 10^4$ Å^3/ns. Total recombination from the contact start $Z = k_c/(4\pi\sigma)$ (− − −) and from minimal separation (—, upper), as well as from remote start distributed with $f_0(D)$ (▲) and from the average initial separation, $\bar{r}(D)$ (△), is shown. The efficiency of the triplet recombination from minimal separation (—, lower), as well as from the distributed starts (■) and from $\bar{r}(D)$ (□), is also shown.

not experience such dramatic changes: the recombination accelerated at slow diffusion passes the maximum and slows down due to spin-conversion control (in region S).

So far we confined ourselves to recombination starting from a single initial separation (the same at any D) that was equalized to either σ or $\bar{r}_{min}$. The results were shown in Figure 7 by dashed and solid lines, respectively. Now we turn to the initial conditions changing with D and represent the results by either filled points when initial separations are distributed according to $f_0(r)$ or empty ones when the start is taken from a single distance $\bar{r}(D)$ (averaged over $f_0(r)$, which is different at any D).

Our calculations address the situation when

$$D = \tilde{D} = \frac{T}{6\pi\sigma\eta} \tag{4.1}$$

In fact, the ion diffusion in polar solvents is a bit slower than that of the neutral reactants and their relationship to viscosity

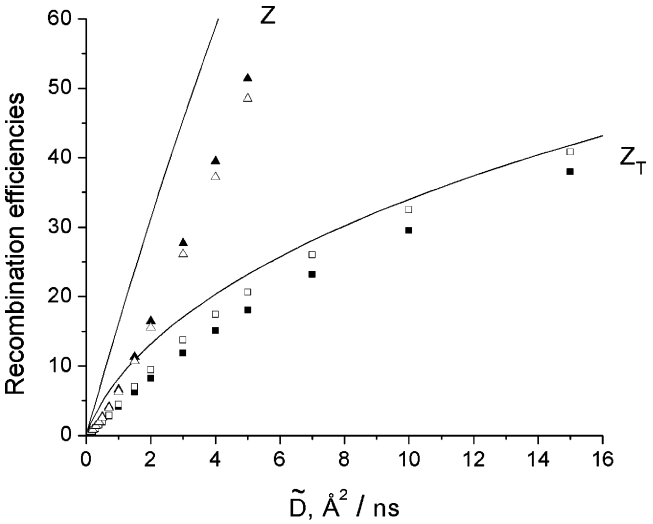

Figure 8. The efficiencies of recombination from different starts at $k_c^S = k_c^T = k_c = 5 \times 10^4$ Å^3/ns in slow diffusion domain. Total recombination from minimal separation (—, upper), as well as from remote start distributed with $f_0(D)$ (▲) and from the average initial separation, $\bar{r}(D)$ (△), is shown. The efficiency of the triplet recombination from minimal separation (—, lower), as well as from the distributed starts (■) and from $\bar{r}(D)$ (□), is also shown.

η, used actually and previously,[8] differs a bit from the Stokes−Einstein expression in eq 4.1. The latter has just to emphasize that D and $\tilde{D}$, changing with viscosity, affect simultaneously both the integrands in eq 1.2, $\varphi(\tilde{D})$ and $f_0(D)$. The results obtained are specific to particular $D = \tilde{D}$ changing with viscosity.

As was expected, the average yield, $\bar{\varphi}$, and the yield from the average separation, $\varphi(\bar{r})$, are not identical, as well as the corresponding efficiencies. However, the difference between Z calculated from the former (●) and from the latter (○) is not pronounced. Similarly Z_T calculated from the distributed starts (▲) and their average value (△) do not differ too much. Moreover, the points do not deviate significantly from the solid curves calculated for the fixed start from $\bar{r}_{min}$. However, this statement is only valid for the fast diffusion limit when recombination is under kinetic or spin-conversion control and $\bar{r}$ has already approached $\bar{r}_{min}$. Along with it, Z approaches its upper limit, which is the plateau of the height

$$\lim_{\tilde{D}\to\infty} Z = \frac{k_c}{4\pi\bar{r}_{min}}$$

This plateau is a bit lower than that shown by the dashed line, which is peculiar for the constant start ($k_c/(4\pi\sigma)$).

The situation is rather different in the opposite limit of slow diffusion, which is mainly studied experimentally. There the total efficiency of diffusional recombination from the fixed start should be linear in $\tilde{D}$, as it really is for $r_0 = \bar{r}_{min}$ (upper solid line in Figure 8). However, the true start at such diffusion is far away from the near contact region and moves toward it when diffusion increases. Therefore the points representing recombination from either distributed (●) or average (○) initial separation lie far below this line. Hence, the diffusional acceleration of total recombination is actually less efficient for remote starts, drawing near with diffusion, than for the fixed and the closest one. Qualitatively the same happens to triplet efficiency: all related points are below the lower solid line, though those calculated from average (△) initial separation are closer to it than those from distributed (▲) initial separation.

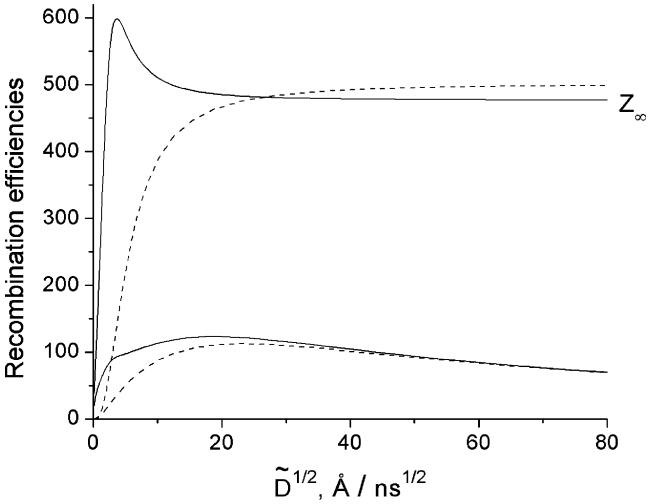

Figure 9. The total (above) and triplet (below) efficiencies of recombination obtained with contact (− − −) and exponential (—) approximations of the recombination layer.

V. Remote Start and Remote Recombination

As a matter of fact, there are no grounds to consider recombination as contact, except the simplicity of the yields calculation. There is the unified theory recipe given in ref 10 (section IX E) how to calculate the averaged yields,

$$\bar{\varphi}_S = \int \varphi_S(r') f_0(r')\, d^3r' \qquad \bar{\varphi}_T = \int \varphi_T(r') f_0(r')\, d^3r'$$
$$\bar{\varphi} = 1 - \bar{\varphi}_S - \bar{\varphi}_T \quad (5.1)$$

expressed via the partial yields of the singlet and triplet recombination products

$$\varphi_S(r') = \int W_S(r) \tilde{p}_{SS}(r,r',0)\, d^3r \quad \text{and}$$
$$\varphi_T(r') = \int W_T(r) \tilde{p}_{ST}(r,r',0)\, d^3r \quad (5.2)$$

that can be found at any $W_S(r)$ and $W_T(r)$. All that we need is the Laplace transformations of the Green functions $\tilde{p}_{SS}(r,r',s)$ and $\tilde{p}_{ST}(r,r',s)$, which obey the set of equations for RIPs subjected to spin conversion and remote double channel recombination (eqs 9.27 in ref 10):

$$-\delta(r-r')/(4\pi r^2) + s\tilde{p}_{SS} = k_s\tilde{p}_{ST} - 3k_s\tilde{p}_{SS} + \mathbf{L}\tilde{p}_{SS} - W_S(r)\tilde{p}_{SS} \quad (5.3a)$$

$$s\tilde{p}_{ST} = -k_s\tilde{p}_{ST} + 3k_s\tilde{p}_{SS} + \mathbf{L}\tilde{p}_{ST} - W_T(r)\tilde{p}_{ST} \quad (5.3b)$$

The encounter diffusion operator

$$\mathbf{L} = \tilde{D}\frac{1}{r^2}\frac{\partial}{\partial r} r^2\, e^{r_c/r}\frac{\partial}{\partial r} e^{-r_c/r}$$

should be used in eqs 5.3a,b together with the reflecting boundary conditions. Solving these equations for only highly polar solvents, we ignored the Coulomb interaction, setting to zero the Onsager radius r_c.

The results presented in Figure 9 were actually obtained using the program Qyield developed by Dr. Krissinel (see http://www.fh.huji.ac.il/ krissinel/software.html). It allows the straightforward calculation of the singlet and triplet pair densities, obeying the set:

$$\dot{m}_S = k_s m_T - 3k_s m_S + \tilde{D}\frac{1}{r^2}\frac{\partial}{\partial r} r^2\, e^{r_c/r}\frac{\partial}{\partial r} e^{-r_c/r}\, m_S - W_S(r)m_S + W_I^S n(r,t) N_S \quad (5.4a)$$

$$\dot{m}_T = -k_s m_T + 3k_s m_S + \tilde{D}\frac{1}{r^2}\frac{\partial}{\partial r} r^2\, e^{r_c/r}\frac{\partial}{\partial r} e^{-r_c/r}\, m_T - W_T(r)m_T \quad (5.4b)$$

identical to eqs 9.6 from ref 10 but with reflecting boundary conditions (and $m_S(0) = m_T(0) = 0$). Here n and N borrowed from eqs 3.2 and 3.4 determine also the initial RIP distributions eqs 3.1 or 3.5. Taking the integrals

$$\phi_S(r') = \int_0^\infty \int W_S(r) m_S(r,t)\, d^3r\, dt = \psi\bar{\varphi}_S,$$
$$\phi_T(r') = \int_0^\infty \int W_T(r) m_T(r,t)\, d^3r\, dt = \psi\bar{\varphi}_T$$

we get the photoionization yields of the singlet and triplet products. They differ from $\bar{\varphi}_S$ and $\phi_T(r')$ by only the multiplier

$$\psi = c\int m_0(r)\, d^3r = \frac{c\kappa\tau}{1 + c\kappa\tau} = 1 - \eta \quad (5.5)$$

which is the RIP yield related to the fluorescence yield η and Stern−Volmer constant as usual.[10]

The recombination rates are usually more extended than the ionization one due to the larger exergonicity of the backward electron transfer. To account for this feature using the exponential models (eq 1.7), we assumed that

$$l_R > l_I \quad (5.6)$$

Under this condition, the total efficiency of remote recombination is a non-monotonous function of diffusion (red line in Figure 9), contrary to what was obtained in the contact approximation (the blue line there). This is due to diffusional deceleration, following the diffusional acceleration of the recombination. At the greatest diffusion, the initial ion distribution coincides in shape with $W_I(r)$.[10] Under condition 5.6, it appears to be narrower than the recombination layer common for the singlet and triplet exponential rates (eq 1.7). Therefore the recombination is weaker the faster the ions get rid of this layer interior. Passing the maximum, the total recombination efficiency Z shown by the red line falls off with the further increase of $\tilde{D}$.

Finally it approaches the plateau, which is lower than the kinetic one reached in the contact approximation (blue line). This pseudo-kinetic value, Z_∞, can be found from the fast diffusion approximation for $\bar{\varphi}$:

$$\bar{\varphi} \approx \frac{\int \varphi(r) W_I(r)\, d^3r}{\int W_I(r)\, d^3r} = 1 - \frac{Z_\infty}{\tilde{D}} \quad \text{at} \quad \tilde{D} \to \infty \quad (5.7)$$

where $\varphi(r)$ is given by expansion 3.5 in ref 21 valid for a single-channel recombination:

$$\varphi(r) = 1 - x\frac{1 + 2\lambda + 2\lambda^2 - \lambda(1 + \delta + 2\lambda)\, e^{-\delta/\lambda}}{1 + \delta} \quad (5.8)$$

Here

$$x = k_c/k_D, \quad \lambda = l_R/2\sigma, \quad \delta = (r - \sigma)/\sigma$$

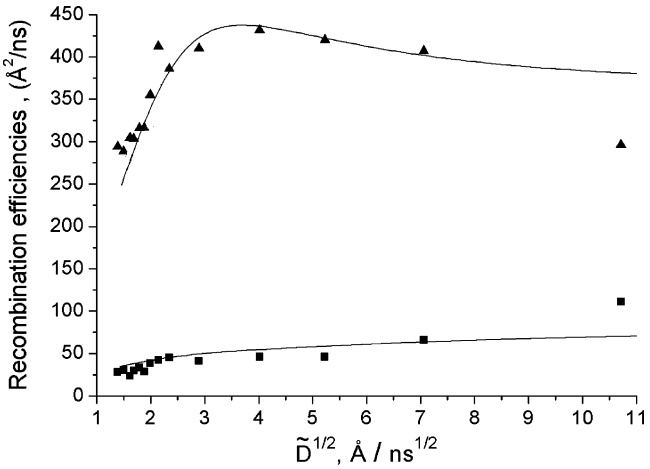

Figure 10. Fitting the theoretical efficiencies (—) to the real experimental data for total (▲) and triplet (■) recombination efficiencies, using the exponential models for both ionization and recombination rates. Parameters obtained from the best fit are the following: $W_i = 29.12\ ns^{-1}$, $W_s = 77\ ns^{-1} = 1.2W_t$, $l_l = 0.81$ Å, $l_R = 1.24$ Å, $k_s = 0.75\ ns^{-1}$, and $\sigma = 7.5$ Å. Analogous to Figure 3.75 in the ref 19.

where $k_c = \int W_S(r)\ d^3r$ is the singlet recombination constant, while the diffusional recombination constant $k_D = 4\pi\sigma\tilde{D}$, as usual. Although this expression was derived for only the singlet recombination at fast diffusion, it is applicable to our double channel model as well, since as $\tilde{D} \to \infty$ the triplet recombination being under spin-conversion control is finally switched off. As follows from eqs 5.7 and 5.8

$$Z_\infty = \frac{W_s\sigma^2 l_R}{(1 + 2\lambda_I + 2\lambda_I^2)l_I}\int_0^\infty [1 + 2\lambda + 2\lambda^2 - \lambda(1 + \delta + 2\lambda)\, e^{-\delta/\lambda}]\, e^{-\delta/\lambda_I}(1 + \delta)\, d\delta \quad (5.9)$$

where $\lambda_I = l_l/(2\sigma)$. Z_∞ is the height of the red plateau, which is really a bit lower than the blue one, appearing in the contact approximation: $\lim_{D\to\infty} Z = k_c/(4\pi\bar{r}_{min})$.

However, the principle difference between remote and contact recombination is seen only in the slow diffusion limit. There the high peak in Z and related increase in Z_T makes it more flat near the maximum. Since this diffusion region is the same as in real systems, it is worthy of special attention. In Figure 10, we see these very features first subjected to experimental and theoretical study in ref 8 but given preliminary noncontact interpretation only in ref 19, For better fitting, we did not assume W_s equal to W_t but took $W_s = 1.2W_t$. Only at the greatest diffusion, the experimental points deviate a bit from the theoretical curves, but all the rest are fitted quite well.

VI. Conclusions

Such an excellent fitting does not prove that the theory is actually the best. There are two essential weaknesses that we hope to eliminate in the near future.

- The exponential models for the ionization and recombination rates should be substituted by the Marcus formulas for these rates, which relate them to the true free energies of the reactions, as well as to the reorganization energy in a particular solvent.
- The true hyperfine interaction mechanism of spin conversion should be substituted for the phenomenological rate model of spin transitions in the RIP.
- The difference in size and encounter diffusion coefficients of ions and their neutral precursors should be taken into account especially in polar solvents.

Hopefully these improvements will enable the theory to correspond better with the fast diffusion experiments and relate the spin-conversion rate to the true values of the hyperfine interaction in particular radicals. However, this will not change our main conclusions:

- The contact reaction approximation can be reasonable for only heavy particles and proton transfer in liquids, whereas the electron transfer either forward or backward is not contact.
- The shape and width of the remote transfer rates strongly affect the yields of reaction products, changing essentially their diffusional dependence.

The unified encounter theory is the universal instrument for investigation of any transfer at any diffusion rate.

References and Notes

(1) Schulten, K.; Staerk, H.; Weller, A.; Werner, H.-J.; Nickel, B. *Z. Phys. Chem. (Frankfurt/Main)* **1976**, *101*, 371.
(2) Schulten, Z.; Schulten, K. *J. Chem. Phys.* **1977**, *66*, 4616.
(3) Werner, H.-J.; Staerk, H.; Weller, A. *J. Chem. Phys.* **1978**, *68*, 2419.
(4) Weller, A.; Nolting, F.; Staerk, H. *Chem. Phys. Lett.* **1983**, *96*, 24.
(5) Weller, A.; Staerk, H.; Treichel, R. *Faraday Discuss. Chem. Soc.* **1984**, *78*, 271.
(6) Michel-Beyerle, M. E.; Haberkorn, R.; Bube, W.; Steffens, E.; Schrëder, H.; Neusser, H. J.; Schlag, E. W. *Chem. Phys.* **1976**, *17*, 139.
(7) Brocklehurst, B. *Chem. Phys. Lett.* **1974**, *28*, 357.
(8) Gladkikh V. S.; Burshtein A. I.; Angulo G.; Grampp G. *Phys. Chem. Chem. Phys.* **2003**, *5*, 2581.
(9) Steiner, U. E.; Ulrich, Th. *Chem. Rev.* **1989**, *89*, 51.
(10) Burshtein A. I. *Adv. Chem. Phys.* **2000**, *114*, 419.
(11) Burshtein, A. I.; Neufeld, A. A. *J. Phys. Chem. B* **2001**, *105*, 12364.
(12) Neufeld, A. A.; Burshtein, A. I.; Angulo, G.; Grampp, G. *J. Chem. Phys.* **2002**, *116*, 2472.
(13) Angulo, G.; Grampp, G.; Neifeld, A.; Burshtein A. I. *J. Phys. Chem. A* **2003**, *107*, 6913.
(14) Burshtein, A. I.; Krissinel, E. *J. Phys. Chem. A* **1988**, *102*, 516.
(15) Burshtein, A. I. *Chem. Phys. Lett.* **1992**, *194*, 247.
(16) Dorfman, R. C.; Fayer, M. D. *J. Chem. Phys.* **1992**, *96*, 7410.
(17) Kilin, S. F.; Mikhelashvili, M. S.; Rozman I. M. *Opt. Spectrosc.* **1964**, *16*, 576.
(18) Steinberg, I. Z.; Katchalsky E. *J. Chem. Phys.* **1968**, *48*, 2404.
(19) Burshtein, A. I. *Adv. Chem. Phys.* **2004**, *129*, 105.
(20) Krissinel, E. B.; Agmon, N. *J. Comput. Chem.* **1996**, *17*, 1085.
(21) Burshtein, A. I.; Zharikov, A. A.; Shokhirev, N. V. *J. Chem. Phys.* **1992**, *96*, 1951.